

Decoupled rolling, sliding and sticking of a viscoplastic drop on a superhydrophobic surface

Minyoung Kim¹, Eungjun Lee², Do Hyun Kim^{2,†} and Rhokyun Kwak^{3,4,†}

¹Department of Chemical Engineering, The Pennsylvania State University, University Park, PA 16802, USA

²Department of Chemical and Biomolecular Engineering, Korea Advanced Institute of Science and Technology, Daejeon 34141, South Korea

³Department of Mechanical Engineering, Hanyang University, Seoul 04763, South Korea

⁴Institute of Nano Science and Technology, Hanyang University, Seoul 04763, South Korea

(Received 27 December 2019; revised 5 October 2020; accepted 13 October 2020)

While the dynamics of Newtonian fluid drops on an inclined non-wettable surface has been widely reported, that of viscoplastic drops is less well known. Combining experimental and theoretical analysis, we reveal unique behaviours of viscoplastic drops on an inclined superhydrophobic surface: (i) decoupled rolling, sliding and sticking motions and (ii) two distinct rolling modes, i.e. viscous rolling and rigid-body rolling. First, determined by the relative magnitudes of gravitational, yield and adhesive stresses, a viscoplastic drop rolls, slides or sticks on a superhydrophobic surface. To the best of our knowledge, this is the first distinct differentiation of viscoplastic drop motions on a superhydrophobic surface, which is a clear departure from the previous observations of Newtonian drops on superhydrophobic surfaces and viscoplastic drops on hydrophilic/hydrophobic surfaces. We subcategorized two types of rolling as liquid-like viscous rolling and solid-like rigid-body rolling. With a low Deborah number (i.e. dimensionless viscoplastic relaxation time), the viscoplastic drop shows a viscous rolling as a Newtonian drop does on an inclined surface. With a high Deborah number, however, the viscoplastic drop does not have enough time to be ‘fluid’. Consequently, the ellipsoidal drop deforms to be more spherical as it goes down the inclined surface, and tumbles, as if a solid body initiates its rolling by ‘tipping’.

Key words: drops, rheology, plastic materials

1. Introduction

In daily life, we deal with various non-Newtonian fluids such as toothpastes, cosmetics, cements, muds, ketchups and gels that can be categorized as viscoplastic fluids. The most important property of these fluids is that they behave like a fluid only if an applied stress is beyond a critical stress (i.e. yield stress), below which they behave like a solid (Balmforth, Frigaard & Ovarlez 2014; Coussot 2014). With broad applications in industries, extensive researches have been conducted to understand the behaviours of viscoplastic fluids. Above all, a better understanding of the interaction of viscoplastic fluids with solid surfaces is

† Email addresses for correspondence: dohyun.kim@kaist.edu; rhokyun@hanyang.ac.kr

critical in environmental situations as well as industries, such as coating, food processing, spraying, inkjet printing, lava flows and landslides. Therefore, many studies have been reported so far, regarding interfacial hydrodynamics such as wetting (Boujlel & Coussot 2013; Jalaal, Balmforth & Stoeber 2015; Jorgensen *et al.* 2015; Varagnolo *et al.* 2015), wall slip (Jalaal *et al.* 2015; Varagnolo *et al.* 2015; Zhang *et al.* 2017, 2018) and drop impact (Luu & Forterre 2009; Oishi, Thompson & Martins 2019; Sen, Morales & Ewoldt 2020). However, the prediction of viscoplastic fluid motions still remains challenging due to the complex nature of the problem with many related factors including yield stress, surface adhesion, surface tension, shear-dependent viscosity, etc. (Balmforth *et al.* 2014; Coussot 2014).

One way to characterize viscoplastic fluids is to focus on the interaction of these fluids and an inclined solid surface. This situation is not only a common experience in engineering processes (e.g. coating processes) and nature (e.g. sliding drops on a window), but it also serves as an effective testbed for controlling various external factors such as gravitational stress, surface adhesion and rheological properties of materials (Mahadevan & Pomeau 1999; Richard & Quéré 1999; Podgorski, Flesselles & Limat 2001; Kim, Lee & Kang 2002; Rio *et al.* 2005; Sakai *et al.* 2006; Suzuki *et al.* 2007; Hao *et al.* 2010; Varagnolo *et al.* 2013; Musterd *et al.* 2014; Schellenberger *et al.* 2016). Recent experimental (Jalaal *et al.* 2015; Varagnolo *et al.* 2015) and numerical (Varagnolo *et al.* 2015) studies revealed that the degree of sliding behaviours of viscoplastic drops depends on surface properties. For example, if the adhesion between a viscoplastic fluid and a solid surface is not strong enough, the attachment of polymer chains on the solid surface would break easily, resulting in the slip on the surface (Balmforth, Craster & Sassi 2002; Coussot *et al.* 2002; Ancey 2007; Chambon, Ghemmour & Naaïm 2014; Zhang *et al.* 2017). While these previous works described some specific behaviours of viscoplastic fluids on surfaces, a basic understanding of the wettability of viscoplastic fluids, such as adhesion and slip conditions, still remains unclear. The complex drop motions of viscoplastic drops and large contact angle hysteresis from the strong surface adhesion on both hydrophilic and hydrophobic surfaces make the understanding of their wetting dynamics difficult. Even the most basic motions of a drop on a solid surface – rolling, sliding and sticking – are difficult to predict, and no one could observe the three basic motions separately on an identical surface.

In this paper, we demonstrate for the first time that a superhydrophobic surface can decouple the rolling, sliding and sticking motions of a viscoplastic drop. With the extremely low surface energy of the superhydrophobic surface, an adhesive stress at the liquid–solid interface is similar in its magnitude to gravitational stress and yield stress. Such a balance of stresses induces the clear decomposition of three basic motions according to their relative magnitudes. In addition, we capture two distinct rolling modes, i.e. liquid-like viscous rolling (Richard & Quéré 1999) and solid-like rigid-body rolling (Hu 2011), as a unique behaviour of a viscoplastic fluid which has not been reported with a Newtonian fluid. Above a critical Deborah number, the viscoplastic drop deforms rather than flows, and it tumbles like a rigid body. On the other hand, with a lower Deborah number, the whole region of the drop is yielded, resulting in a tank-treading viscous rolling as in Newtonian fluid drops (Richard & Quéré 1999).

2. Methods and materials

2.1. Experimental set-up

A schematic of a viscoplastic drop on an inclined superhydrophobic surface is shown in [figure 1](#). The superhydrophobic surface was fabricated by coating paraffin-wax-fixed

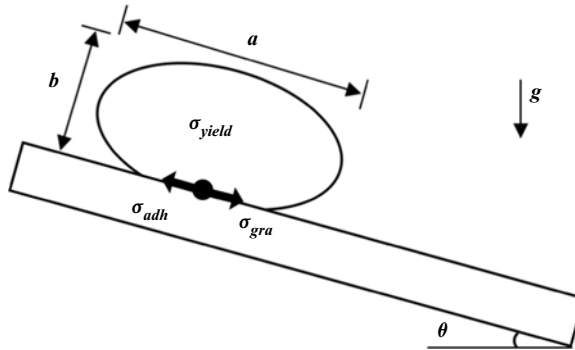


FIGURE 1. Schematic of the experiment. Xanthan gum solution drops (0.25–2.5 wt%) are placed on a superhydrophobic surface. Each drop has a diameter a and a height b . The gravitational (σ_{gra}), yield (σ_{yield}) and adhesive (σ_{adh}) forces (stresses) are taken into consideration in the observation of rolling, sliding and sticking behaviours.

candle soot on a glass slide (static contact angle of deionized water: $162 \pm 2^\circ$) (Seo, Kim & Kim 2014). Viscoplastic fluids were prepared by mixing xanthan gum powder (0.25–2.5 wt%; Sigma-Aldrich) into deionized water for 24 h at 300 rpm, 25°C . The solution was then kept at 4°C for 12 h to finish biopolymer hydration (Jaishankar & McKinley 2014). The resultant xanthan gum solutions had controllable viscoplasticity with respect to their concentration as well as high thermal stability and biocompatibility (Whistler & BeMiller 1993; Song, Kim & Chang 2006).

The targeting volume of the released drop was $250 \mu\text{l}$ (minimum tilting angle of a $250 \mu\text{l}$ water drop $< 1^\circ$). For dispensing a drop of low concentration of xanthan gum (≤ 0.5 wt%), there was no residue at the pipette. For high concentrations (> 0.5 wt%), however, the fluid was not completely detached from the pipette. Therefore, we monitored the drop dimensions so that the experimental results outside of an acceptable range of $250 \pm 30 \mu\text{l}$ (which corresponds to a diameter of 9.7 ± 1.1 mm and a height of 4.4 ± 0.2 mm; a and b in figure 1) were avoided. Regarding the durability of the surface and its contamination, we did not observe a certain change of contact angles in our experiments, which is typical evidence of a wetting transition in a macroscopic view. Indeed, Seo *et al.* (2014) carried out two tests to show the mechanical durability of the surface: (i) jetting water onto the surface with a dispenser bottle, resulting in a water pressure of $\sim 25\,000$ Pa from ρV^2 , where V is the impact velocity of water scaled as 5 m s^{-1} and (ii) water drop impact with a height of 10–60 cm resulting in a water pressure of $\sim 50\,000$ Pa from $\rho V^2 = \rho gh$, where g and h are the acceleration of gravity ($\sim 10 \text{ m}^2 \text{ s}^{-1}$) and height (~ 0.5 m). Since the surface was robust enough to resist 50 000 Pa, a $250 \mu\text{l}$ drop for our experimental conditions is not enough to push (by its weight) the substrate and cause a wetting transition; the corresponding water pressure on the surface is only ~ 40 Pa (equal to the hydrostatic pressure of the drop, $b\rho g$).

The drop motions were monitored along the inclined surfaces (46 mm in length) using a contact angle analyser (Phoenix 300, SEO, South Korea). To check the reproducibility, the experiments were repeated three times, and it was confirmed that the drops show the same behaviour. The drop height corresponds to $2\kappa^{-1}$, where κ^{-1} is the capillary length (de Gennes, Brochard-Wyart & Quéré 2013), and thus the drop shapes were flattened by gravity. The coffee particles and/or bubbles inside the drops were traced to confirm

drop motions. The inclined angle of the surface (θ) was changed in the range 1.1–17.5°. The advancing and receding angles of the viscoplastic drop on the inclined surface, $161 \pm 3^\circ$ and $156 \pm 3^\circ$, respectively, were almost the same for various inclined angles and xanthan gum concentrations. This indicates that the variation of surface tension and contact angle hysteresis among xanthan gum solutions with different concentrations is negligible (Varagnolo *et al.* 2015).

2.2. Determination of adhesive stress

For identical superhydrophobic surface and corresponding fixed surface energy, the adhesive stress was controlled by the xanthan gum concentration. At the initial condition immediately after the release of the drop on the surface, we assumed the viscoplastic fluid as an elastic rubber. The elastic modulus ($G = 10^3 cRT/M_e$) and the molecular weight between entanglements ($M_e = k_1/c$) can be combined to form the proportional relationship between G and c^2 : $G = 10^3 c^2 RT/k_1$, where k_1 is a constant ($1.7 \times 10^4 \text{ kg}^2 \text{ m}^{-3} \text{ mol}^{-1}$), c is the concentration of xanthan gum (kg m^{-3}), R is the gas constant and T is the temperature (Horinaka, Tanaka & Takigawa 2015). Here, the adhesive stress between solid and polymeric liquid can be expressed as $\sigma_{adh} = G\gamma^*(A_R/A_0)$, where γ^* is the critical shear strain at which the detachment of entangled polymer chains occurs on the surface, A_R is the real contact area and A_0 is the apparent contact area. The ratio A_R/A_0 is much smaller than unity because the superhydrophobic surface is generally very rough (de Gennes *et al.* 2013). When a shear stress is large enough, the chains attached to the solid surface are stretched, and the adhesive links start to break at the critical strain. If the solid surface has a higher surface energy, a larger shear stress and deformation would be required to break the links. In this work, we assumed γ^* and A_R/A_0 are constant because the same polymer and surface were used for all experiments, so the adhesive stress σ_{adh} is only varied by c^2 . To demonstrate this relationship and to determine the constant $\gamma^*(A_R/A_0)$, we performed an experiment for one concentration of xanthan gum and observed the drop behaviour so that the adhesive stress can be evaluated as an external force in the horizontal direction of the inclined plane (i.e. gravitational stress) at the moment the drop starts to slide. From our experiment, a drop of 1 wt% concentration sticks and slides on the surface at 1 and 2 Pa, respectively. Thus, the adhesive stress at this concentration was able to be assumed as 1.5 Pa, and the constant $\gamma^*(A_R/A_0)$ was calculated as 10^{-4} . As a result, the adhesive stress can be derived as $\sigma_{adh} \approx 0.1c^2RT/k_1$.

2.3. Determination of yield stress

For the measurement of the yield stress of xanthan gum solutions, two different tests were performed with rotational rheometers: (i) measuring a shear rate in time at a given shear stress (also known as a creep test) with parallel plates covered with sandpaper (AR-G2, TA Instruments) and (ii) measuring a shear stress with increasing shear rate using a smooth cone-and-plate geometry (HAKKE MARS, Thermo Electron GmbH). In all measurements, fresh (not pre-sheared) sample solutions were used which had a resting time of more than 12 h after the preparation of solutions and 5 min after loading on the rheometer. The detailed description and experimental results are given below.

2.3.1. Creep tests of xanthan gum solutions

First, we performed creep tests to measure the yield stress of xanthan gum solutions of 0.5, 1.0, 1.5, 2.0 and 2.5 wt% (figure 2). In these tests, shear rate responses were monitored

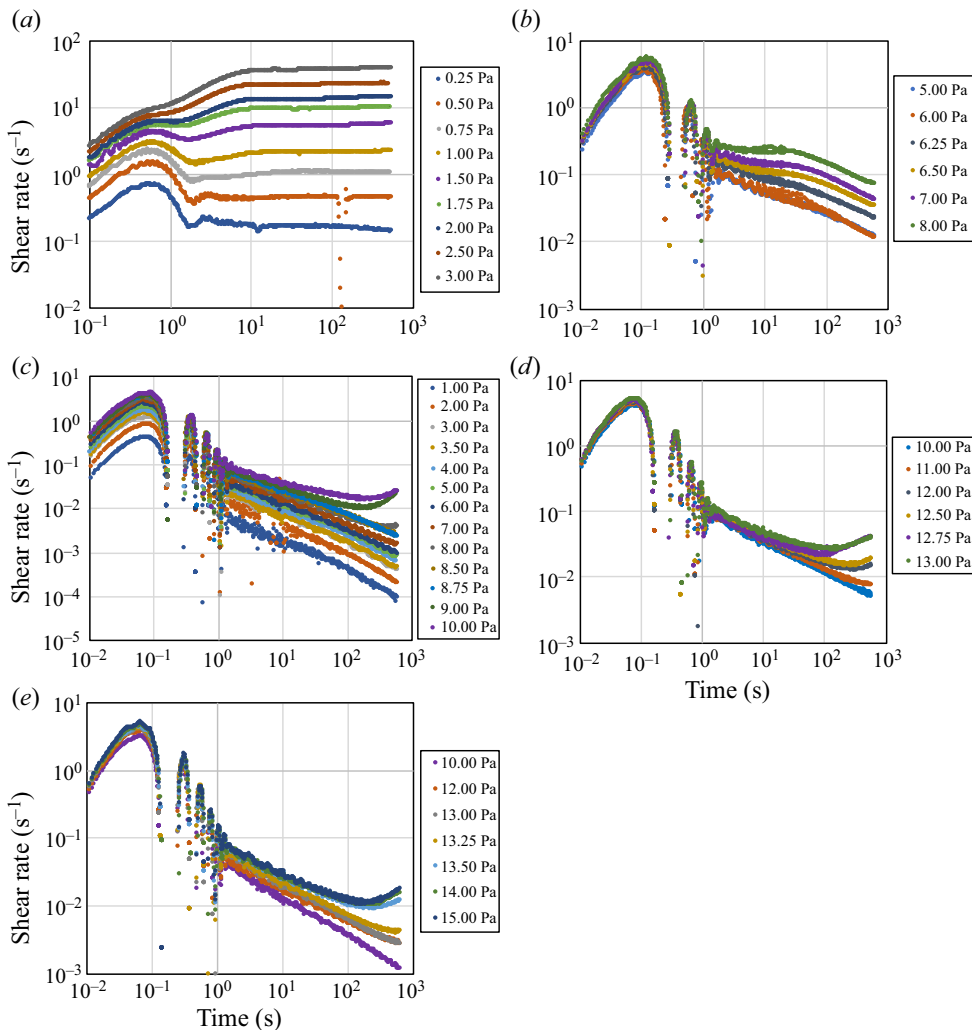


FIGURE 2. Creep tests for xanthan gum solutions of (a) 0.5 wt%, (b) 1.0 wt%, (c) 1.5 wt%, (d) 2.0 wt% and (e) 2.5 wt%.

during 1000 s at a given applied shear stress in the range 0.25–15 Pa. Parallel plates (1 mm gap) coated with sandpaper were used so that the two following possible experimental artefacts were eliminated: (i) the wall slip by performing the rheological measurements on rough surfaces (Balmforth *et al.* 2014) and (ii) the residual effect by applying a shear stress to a viscoplastic fluid and observing its deformation over time instead of applying a finite amount of shear rate which may result the shear stress response before the full development of the internal flow in the early stage of the shear stress versus shear rate measurement (Dinkgreve, Denn & Bonn 2017).

As can be seen in figure 2(c–e), we can observe a clear bifurcation of the shear rate responses at relatively high concentrations (1.5–2.5 wt%) around 100 s. Based on this bifurcation, the yield stresses can be identified as 8, 12 and 13.3 Pa for 1.5, 2.0 and 2.5 wt% xanthan gum solutions, respectively. At relatively low concentrations (0.5 and 1 wt%), the bifurcation of the shear rate responses can still be observed, but its characteristic is

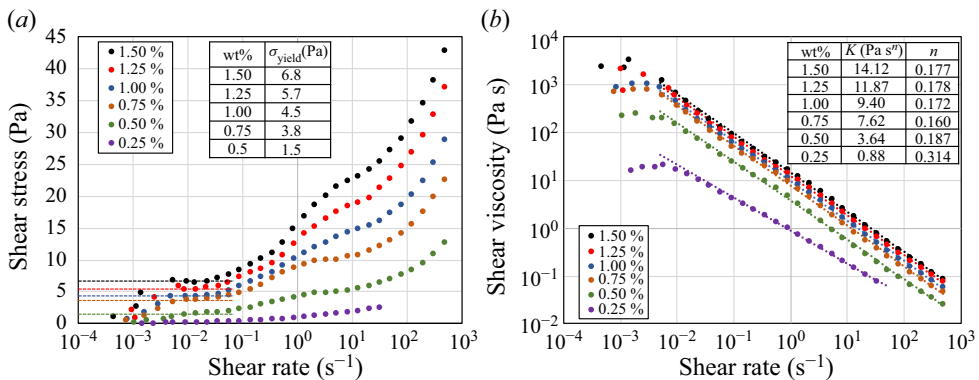


FIGURE 3. (a) Shear stress and (b) shear viscosity of xanthan gum solutions of 0.25–1.5 wt%. (a) The plateau regions of the shear stress are observed in 0.005–0.025 s⁻¹ for 0.5–1.5 wt%, which is expected to be the presence of the apparent yield stress (see the dashed lines and the inset table for the predicted yield stress values). No plateau has been observed for 0.25 wt%. (b) Shear viscosity fitted with the power-law model ($\eta = K\dot{\gamma}^{n-1}$). All data were measured with a cone-and-plate geometry with increasing shear rate with a time interval of 172 s per data point.

somewhat different from that at high concentrations (figure 2a,b). For a concentration of 0.5 wt%, the considerable bifurcation happens immediately before 1 s (figure 2a). A decrease of the shear rate response is observed below a shear stress of 1.5 Pa, whereas a constant or an increase in the shear rate is observed above 1.75 Pa. This bifurcation may have the same physical origin as the bifurcation phenomena at higher concentrations (1.5–2.5 wt%). The later behaviour is probably explained by the shear rejuvenation, which is due to the abrupt decrease in the viscosity of thixotropic yield stress fluids (Coussot & Ovarlez 2010). In addition, since uniform stress cannot be applied within the parallel plate geometry, we expect that some parts of the sample are yielded and the others are not; thus, shear banding may occur that causes the constant shear rate response after the shear rejuvenation even below the yield stress (at > 10 s and < 1.5 Pa in figure 2a) (Moller, Mewis & Bonn 2006). For a concentration of 1.0 wt%, a slope difference was found from 1 to 10 s between 6 and 8 Pa of applied shear stress, and this bifurcation point probably indicates the presence of yield stress based on the same analogy as above. However, since we could not find any evidence and reasonable explanation for the same negative slope of the shear rate afterwards, we did not define the yield stress for a concentration of 1.0 wt%. The predicted yield stresses from the creep tests show a good agreement with the data of Song *et al.* (2006) who obtained yield stresses with the Herschel–Bulkley model (figure 4). Of course, since the material is likely to flow before the bifurcation of the shear rate responses (i.e. within the supposed solid regime), it is notable that the measured yield stress here would be an ‘apparent yield stress’ of xanthan gum solutions (not true yield stress).

2.3.2. Shear stress versus shear rate of xanthan gum solutions

To identify the yield stresses of xanthan gum, we additionally measured stress responses of 0.25–1.5 wt% xanthan gum solutions with increasing shear rate from 0.001 to 500 s⁻¹ with a time interval of 172 s per data point (figure 3a). A rheometer equipped with a 1° cone of 60 mm in diameter and a flat plate was used. Both cone and plate have smooth surfaces. As shown in figure 3(a), the plateau regions are observed in 0.005–0.025 s⁻¹

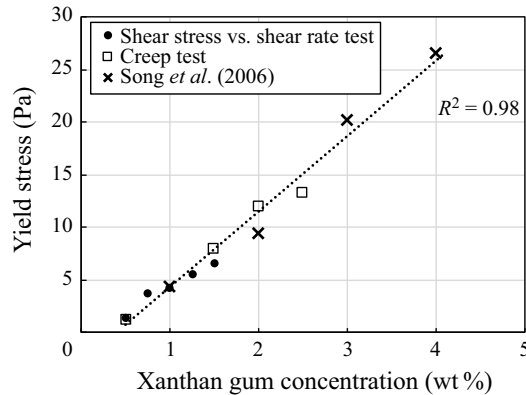


FIGURE 4. Measured yield stresses combined with the results from Song *et al.* (2006) (the yield stress of xanthan gum solutions with the Herschel–Bulkley model). A linear relationship between the yield stress of xanthan gum solutions and the solute concentration is predicted.

for 0.5–1.5 wt% xanthan gum solutions (the shear rate of 0.005 s^{-1} corresponds to 690 s from the beginning of the measurement). Such rheological response has been frequently observed for other viscoplastic fluids such as a Carbopol gel (Mahaut *et al.* 2008) and bentonite suspension (Song *et al.* 2006; Ovarlez *et al.* 2013). Here, we define the ‘apparent yield stress’ as the averaged stress of this plateau region which also follows the data from Song *et al.* (2006) (figures 3*a* (inset table) and 4). Since no plateau has been observed for the xanthan gum solution of 0.25 wt%, we concluded that there is no apparent yield stress for such a low concentration.

Although we successfully identified the apparent yield stress of 0.5–1.5 wt% xanthan gum solutions, the measurement was performed with (1) smooth surfaces and (2) step-increasing shear rate. Therefore, it was not free from the experimental artefacts as we described in § 2.3.1. We presumed that undesirable slip happens at an initial low-shear-rate regime (below 0.005 s^{-1}), resulting in the linear increase of stress responses (figure 3*a*). Also, it was difficult to measure the stress responses for high concentrations (>1.5 wt%) due to the considerable slips.

Finally, through two rheological measurements, the linear relationship between the yield stress and the concentration can be derived as $\sigma_{yield} = k_2(c - c_0)$, where k_2 is a constant ($0.72 \text{ m}^2 \text{ s}^{-2}$) and c_0 is the critical concentration where a finite magnitude of yield stress occurs (2.50 kg m^{-3} ; i.e. x -intercept of $\sigma_{yield}-c$ plot in figure 4). The occurrence of finite magnitude of yield stress at c_0 also matches with the previous work of Wyatt & Liberatore (2009) that reported a critical concentration of 2.0 kg m^{-3} for completely entangled polymer chains of xanthan gum.

3. Results and discussion

3.1. Rolling, sliding and sticking motions of a viscoplastic drop

When the viscoplastic drop was released on the inclined superhydrophobic surface, as shown in figures 5 and 6(*a*), rolling, sliding and sticking motions were differentiated according to the surface inclination and xanthan gum concentration. At a higher inclination and/or lower concentration, the triangle connection of the coffee particles rotated as the drop went down along the surface, indicating rolling ($1.15^\circ/0.25 \text{ wt\%}$ in figure 5*a*

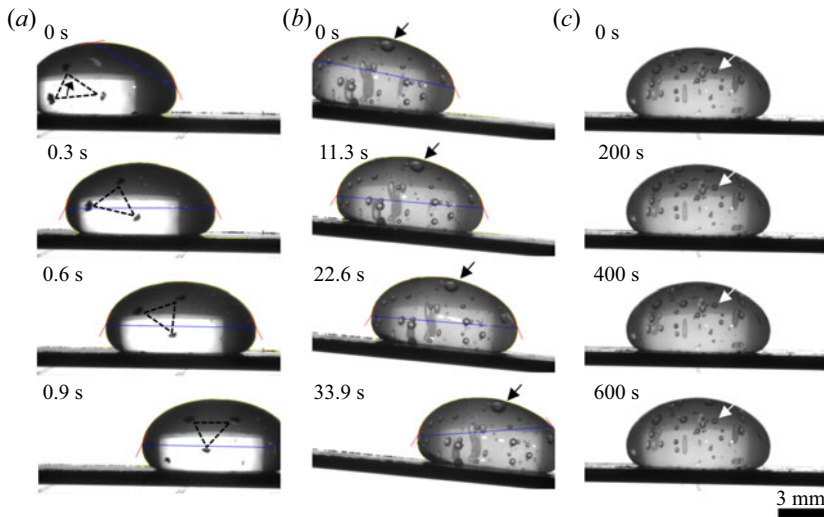


FIGURE 5. Image sequences of (a) rolling, (b) sliding and (c) sticking of the viscoplastic drops. (a) At 1.15° inclination and 0.25 wt% concentration, the connection of the coffee particles (dashed triangle) rotates within the drop, indicating a rolling motion (see supplementary movie 1 available at <https://doi.org/10.1017/jfm.2020.895>). (b) At 5.74° inclination and 1.0 wt% concentration, the air bubbles in the drop show no relative motions inside of the drop, indicating a sliding motion (see supplementary movie 2). (c) At 1.15° inclination and 1.0 wt% concentration, the drop sticks on the surface over 10 min.

and supplementary movie 1). As the inclined angle decreased and/or xanthan gum concentration increased, the drop slid without internal fluid flows ($5.74^\circ/1.0$ wt% in figure 5b and supplementary movie 2). In this case, the tracers moved parallel to the surface, and did not show any relative change of position inside the drop. At a lower inclination and higher concentration, the viscoplastic drop just stuck on the surface, and stayed at the initial location ($1.15^\circ/1.0$ wt% in figure 5c). These unique behaviours of viscoplastic drops due to the yield and adhesive stresses are clearly different from the traditional picture of Newtonian drops on a non-wettable surface (i.e. rolling or sliding without sticking (Mahadevan & Pomeau 1999; Richard & Quéré 1999) and sticking by contact angle hysteresis and/or pinning on hydrophilic surfaces (Musterd *et al.* 2014)) and even from the observations of viscoplastic drops on hydrophilic/hydrophobic surfaces (i.e. mixed rolling–sliding–sticking motions; Jalaal *et al.* 2015; Varagnolo *et al.* 2015) and avalanche behaviours (Coussot *et al.* 2002).

First, we analyse under what conditions viscoplastic drops roll, slide or stick, and why these motions can be decoupled on a superhydrophobic surface. We hypothesize that ratios of the three stresses, $\sigma_{adh}/\sigma_{gra}$ and $\sigma_{yield}/\sigma_{gra}$, determine rolling–sliding–sticking regimes because these two stress ratios govern the detachment of the viscoplastic drop from the surface and the fluidity of the drop, respectively. The adhesive stress and yield stress can be present as $\sigma_{adh} = 0.1c^2RT/k_1$ and $\sigma_{yield} = k_2(c - c_0)$ (as we derived from the rheological measurements). The gravitational stress σ_{gra} can be scaled as $b\rho g \sin \theta$. Then, the relative magnitudes of the stresses are

$$\frac{\sigma_{adh}}{\sigma_{gra}} = \frac{0.1c^2RT}{k_1b\rho g \sin \theta}, \quad \frac{\sigma_{yield}}{\sigma_{gra}} = \frac{k_2(c - c_0)}{b\rho g \sin \theta}. \quad (3.1a,b)$$

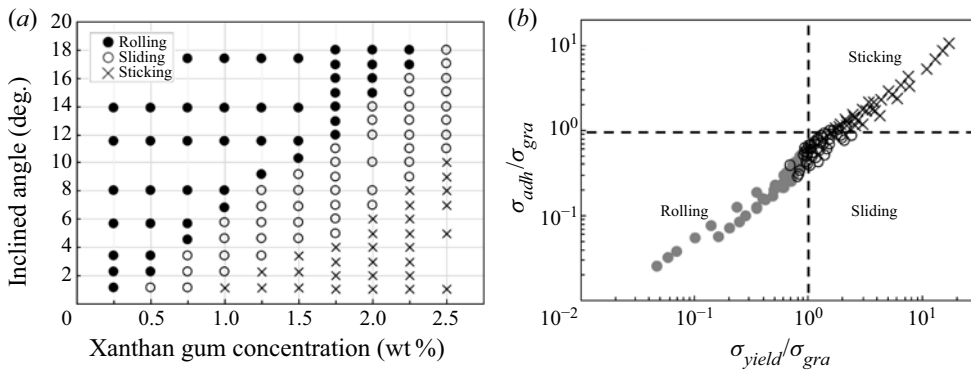


FIGURE 6. (a) Phase diagram of rolling, sliding and sticking as a function of inclined angle and xanthan gum concentration. (b) Phase diagram of drop motions based on two stress ratios.

Figure 6(b) shows the phase diagram of three motions enumerated by the stress ratios. As we expected, the ratio of yield and gravitational stresses ($\sigma_{yield}/\sigma_{gra}$) differentiates rolling and sliding regimes, and the ratio of adhesive and gravitational stresses ($\sigma_{adh}/\sigma_{gra}$) differentiates sticking and sliding motions. In detail, for rolling, the gravitational stress surpasses the other two stresses (filled circles in figure 6b). Accordingly, the drop is detached from the surface ($\sigma_{adh}/\sigma_{gra} < 1$), and also deforms and flows to rotate ($\sigma_{yield}/\sigma_{gra} < 1$). For sliding, whereas the gravitational stress is still beyond the adhesive stress to detach the drop, the drop is not required to be ‘fluid’ ($\sigma_{yield}/\sigma_{gra} > 1$) (open circles in figure 6b). For sticking, the surface should hold the drop without any external ($\sigma_{adh}/\sigma_{gra} > 1$) and internal ($\sigma_{yield}/\sigma_{gra} > 1$) motions (crosses in figure 6b).

In the phase map, three basic behaviours of the viscoplastic drop can be successfully predicted on the superhydrophobic surface. However, even with high concentrations of xanthan gum, we could only cover the half of the plane below $y = x$ (i.e. $\sigma_{adh} < \sigma_{yield}$), due to the low adhesive energy of the superhydrophobic surface. If the viscoplastic drop was on more sticky surfaces, rolling, sliding and sticking motions would not be decomposable. In addition, if $\sigma_{adh} > \sigma_{yield}$, the drop will be able to flow and stick simultaneously, inducing the so-called avalanche behaviour (Coussot *et al.* 2002). So, in quadrant 2 of figure 6(b), the drop sticks at the initial position ($\sigma_{adh}/\sigma_{gra} > 1$), but the upper region of the drop flows as gravity overwhelms the yield stress ($\sigma_{yield}/\sigma_{gra} < 1$).

We have tested other superhydrophobic surfaces covered with hydrophobic silica nanoparticles created by silicone oil combustion (Seo *et al.* 2016), and found rolling, sliding and sticking motions as well. However, since these surfaces were relatively easily broken and contaminated, we could not gather meaningful data sets. Regarding this aspect, we plan to work in the future with a different type of superhydrophobic surface that secures its superhydrophobicity with mechanical structures such as microscale/nanoscale pillars. We expect that varying the dimension of a pillar, pillar interdistance and surface energy might allow us to control the magnitude of the adhesive stress and therefore to investigate in detail the interaction between a viscoplastic fluid and a solid substrate.

3.2. Two distinct rolling modes

In addition to decoupling of rolling, sliding and sticking of a viscoplastic drop, we also identify two rolling modes on the inclined superhydrophobic surface, i.e. viscous

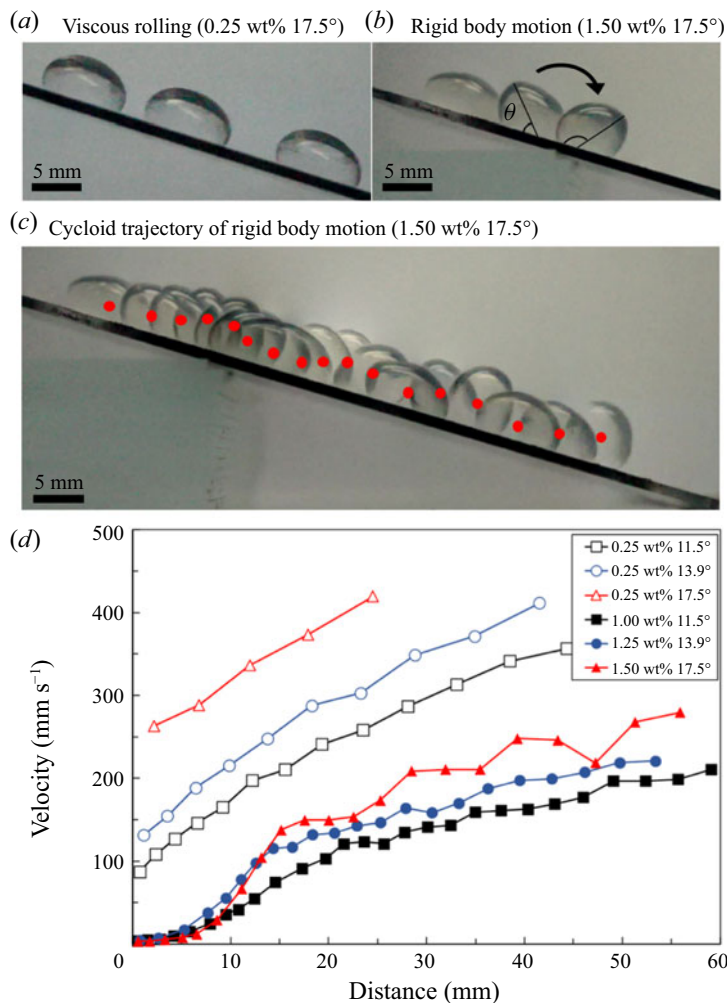


FIGURE 7. (a) Viscous rolling (17.5° and 0.25 wt%) and (b) rigid-body rolling (17.5° and 1.5 wt%) of the viscoplastic drop. (c) The centre of mass of the drop (marked as red circles) shows a cycloid trajectory verifying the rigid-body rolling and subsequently showing the periodic fluctuation in its velocity (d). (d) Distance–velocity profiles of viscous rolling (0.25 wt%; open symbols) and rigid-body rolling (1.0–1.5 wt%; filled symbols) (see supplementary movie 3).

rolling and rigid-body rolling. We expect that these two rolling modes are differentiated depending on whether the drop shifts its shape or not. One of the major differences of viscoplastic fluids from Newtonian ones is the capability of a permanent shift in shape (Luu & Forterre 2009). According to Richard & Quéré (1999), only a spherical viscous drop rolls like a solid on a tilted non-wettable surface. Therefore, the drop should be small enough so as not to be flattened by gravity. In our experiment with a 0.25 wt% xanthan gum solution, we observed a tank-treading rolling as in a Newtonian fluid, and the velocity increased with nearly constant acceleration (figure 7a and open symbols in figure 7d). In the case of highly concentrated xanthan gum solutions (≥ 0.5 wt%), however, even if the initial shape of the drop is an ellipsoid, it can roll like a solid. Of course, to initiate this rigid-body rolling, the viscoplastic drop also needs to change

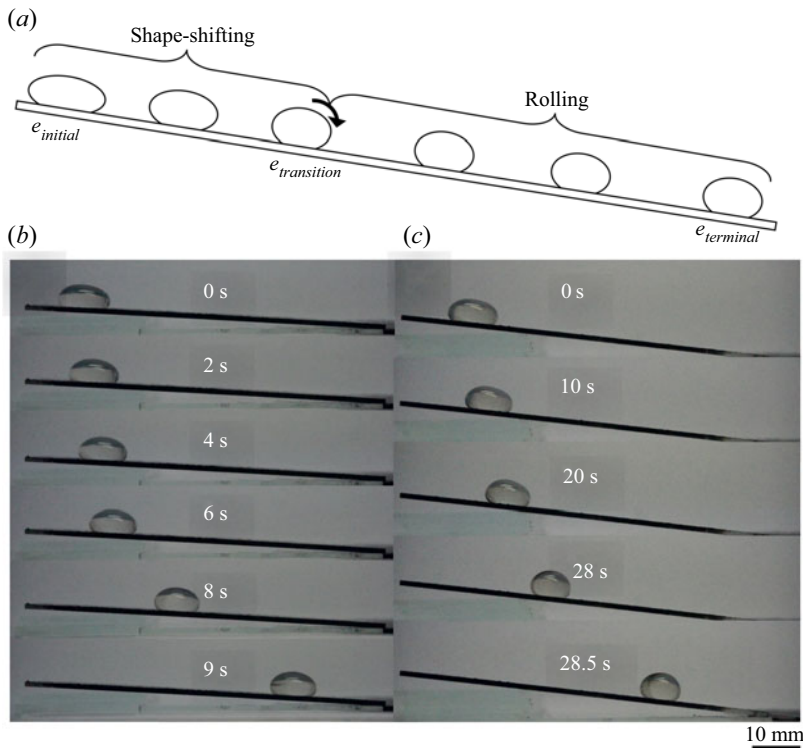


FIGURE 8. (a) Two steps for rigid-body motions: (i) shape shifting (from the initial point where a drop starts to move to the transition point where it starts to accelerate) and (ii) rigid-body rolling (from the transition point to the end of the substrate). Viscoplastic drops mostly change their shape at the initial shape-shifting stage and roll off as a solid with a velocity fluctuation. (b) At 3.44° inclination and 0.5 wt% concentration, the drop slowly moves down for the first 6 s (the shape-shifting stage) and goes through a subsequent fast rolling motion (rigid-body rolling stage). (c) At 6.89° inclination and 1.0 wt% concentration, the drop shows a greater variation in its width and height during the initial shape-shifting stage compared to the case in (b).

its shape to become more spherical and minimize the contact area with the non-wettable surface first. The viscoplastic ellipsoid initially went down the slope with a lower speed (<7 mm distance, filled symbols in figure 7*d*). Then, the drop tipped and started to roll like a rigid body showing a sudden acceleration in velocity which was predicted based on the location where the centre of mass of a drop was projected to the inclined surface (figure 7*b–d*). Specifically, a drop for 17.5° inclination and 1.5 wt% concentration showed an oscillation in velocity (represented as filled triangles in figure 7*d*) and a cycloid trajectory (figure 7*c*) similar to a solid body rolling with a non-uniform mass distribution and/or asymmetric shape (Hu 2011). The location of the increase (decrease) in the acceleration in figure 7(*d*) corresponds to the moment when the distance between the centre of the drop and the substrate decreases (increases). Based on our observations, we define two steps for rigid-body rolling: shape shifting and rigid-body rolling. As shown in figure 8, the viscoplastic drops initially shift their shape while moving down on an inclined superhydrophobic surface with a lower speed and roll off with a higher velocity. One notable feature is that the amount of shape variation depends on experimental

conditions. For example, at 3.44° inclination and 0.5 wt% concentration (figure 8*b*) and 6.89° inclination and 1.0 wt% concentration (figure 8*c*), we noticed that there was a larger variation in the drop shape (i.e. more spherical) for the latter experimental condition (figure 8*c*). Probably, if we released the drop as the major axis of the elliptic drop is aligned vertically to the surface, it may be more feasible to initiate the rigid-body rolling. To preclude such undesirable effects, we carefully released the drop right on the surface as described in supplementary movie 3.

To predict the degree of shape shifting and corresponding rolling modes, we quantified the shape of the viscoplastic drop by measuring an eccentricity ($e = (1 - (b/a)^2)^{1/2}$) at the initial state ($e_{initial}$), transition state between the shape-shifting and rolling stages ($e_{transition}$) and the final state ($e_{terminal}$) (figure 8*a* and table 1). Figure 8(*b,c*) shows that the viscoplastic drop can be deformed more at a higher xanthan gum concentration and/or a higher inclination. Most of the shape change occurred in the shape-shifting stage (as we named), and there was a negligible eccentricity variation afterwards. Based on this measurement of the eccentricity, we performed a scaling analysis to express the degree of shape shifting ($\Delta e = e_{initial} - e_{transition}$) with Deborah number (De), which describes the magnitude of the solidity and/or fluidity of materials (Reiner 1964). This number is defined as the ratio of the relaxation time t_{relax} and the processing time t_{proc} : $De = t_{relax}/t_{proc}$. In rheology, when the time for adjusting to applied stresses or strains (i.e. relaxation time) on a material is greater than the time scale for an experiment (i.e. processing time), it is considered as a solid-like material. Here, the relaxation time represents the required time to set the drop shape by surface tension, and the processing time indicates the residual time to yield the viscoplastic fluids under gravitational stress at the liquid–solid interface. While shape shifting, the gravitational stress deforms the drop and changes its eccentricity over the processing time, and at the same time the Laplace pressure acts on the surface of the drop making it come back to its original shape at the initial state over the relaxation time.

In this scenario, the shape of the drop can be determined based on the ratio of two time scales. If De is large, the viscoplastic drop does not have enough time to circulate the yielded parts of the fluid inside of the drop. Otherwise, if De is small, the whole region of the drop can be yielded with a sufficient processing time, and tank-treading motion might occur as for a Newtonian fluid (Richard & Qu  r   1999). From the hypothesis that the drop is deformed by the gravitational stress in the shape-shifting stage, we write a relation: $\rho\pi(a/2)^2b\Delta x/t_{proc}^2 \sim \pi(a/2)^2(\sigma_{gra} - \sigma_{yield})$. The right-hand-side terms represent the net force for the deformation of the viscoplastic drop with a volume of $\pi(a/2)^2b$ and the left-hand-side terms describe the corresponding drop motion for the processing time. Here, the drop starts to roll like a rigid body after a quarter rotation (figure 9 and supplementary movie 4), so the displacement of the drop Δx can be a quarter of the perimeter of the drop, $(1/4)\pi a$. The processing time is then scaled as

$$t_{proc} \sim \left[\frac{(1/4)\rho\pi ab}{\sigma_{gra} - \sigma_{yield}} \right]^{1/2}. \quad (3.2)$$

For the relaxation process, we set a relation, $\gamma/b \sim \sigma_{yield} + \eta_c/t_{relax}$, and scaled the relaxation time as $t_{relax} \sim \eta_c/(\gamma/b - \sigma_{yield})$, where γ is the surface tension and η_c is the characteristic viscosity that represents the viscosity of the viscoplastic drop at the moment of shape shifting. To this end, first, the characteristic shear rate $\dot{\gamma}_c$ (the shear rate of the drop at the moment of shape shifting) is scaled as $\Delta x/t_{proc}b$ so that $\Delta x/t_{proc}$

Concentration (wt%)	σ_{gra} (Pa)	$e_{initial}$	$e_{transition}$	$e_{terminal}$	$e_{initial} - e_{transition}$	$e_{initial} - e_{terminal}$	$e_{transition} - e_{terminal}$
0.5	3	0.890	0.845	0.856	0.045	0.034	-0.011
	5	0.883	0.835	0.841	0.048	0.042	-0.006
	7	0.895	0.808	0.861	0.087	0.034	-0.053
	10	0.897	0.861	0.856	0.036	0.041	0.005
0.75	4	0.893	0.836	0.819	0.057	0.074	0.017
	5	0.910	0.822	0.823	0.088	0.087	-0.001
	6	0.897	0.803	0.795	0.094	0.102	0.008
	7	0.890	0.792	0.805	0.098	0.085	-0.013
	10	0.917	0.792	0.800	0.125	0.117	-0.008
	12	0.898	0.761	0.837	0.137	0.061	-0.076
1.0	15	0.885	0.770	0.866	0.115	0.019	-0.096
	6	0.894	0.767	0.759	0.127	0.135	0.008
	7	0.861	0.756	0.763	0.105	0.098	-0.007
	8	0.895	0.762	0.782	0.133	0.113	-0.020
	10	0.866	0.771	0.750	0.095	0.116	0.021
	12	0.892	0.766	0.761	0.126	0.131	0.005
1.25	15	0.884	0.687	0.870	0.197	0.014	-0.183
	8	0.861	0.733	0.727	0.128	0.134	0.006
	10	0.851	0.714	0.708	0.137	0.143	0.006
	12	0.884	0.690	0.720	0.194	0.164	-0.030
1.5	15	0.871	0.693	0.752	0.178	0.119	-0.059
	10	0.871	0.649	0.643	0.222	0.228	0.006
	12	0.883	0.629	0.649	0.254	0.234	-0.020
	15	0.881	0.583	0.866	0.298	0.015	-0.283

TABLE 1. The eccentricities and their variations measured at the initial point where a drop starts to move ($e_{initial}$), transition point where a drop starts to accelerate ($e_{transition}$) and terminal point at the end of the substrate ($e_{terminal}$).

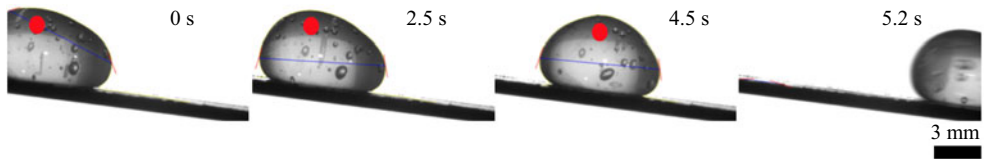


FIGURE 9. After a quarter rotation of the drop for 0–4.5 s (when the red circle initially positioned at the rear side of the drop reaches the top of the drop), it tumbles down on the inclined substrate as a solid body.

Concentration (wt%)	σ_{gra} (Pa)	$\dot{\gamma}_c$ (s^{-1})	η_c (Pa s)
0.5	1	7.93	0.213
	2	11.21	0.168
	3	13.73	0.146
	5	17.73	0.123
	7	20.98	0.109
	10	25.07	0.097
	12	27.47	0.091
0.5	15	30.71	0.084
	3	11.97	0.483
	5	16.40	0.374
	7	19.87	0.320
	10	24.15	0.273
0.75	4	9.68	1.132
	5	12.51	0.912
	6	14.81	0.792
	7	16.80	0.712
	10	21.70	0.575
	12	24.42	0.520
1.0	15	28.02	0.463
	6	10.34	1.359
	7	13.03	1.122
	8	15.25	0.985
	10	18.93	0.824
1.25	12	22.00	0.727
	15	25.94	0.635
	8	10.96	1.659
	10	15.68	1.236
1.5	12	19.27	1.043
	15	23.67	0.881
	10	11.54	1.886
1.5	12	16.09	1.435
	15	21.15	1.146

TABLE 2. The characteristic shear rate $\dot{\gamma}_c$ and viscosity η_c predicted from the power-law relationship in figure 3(b).

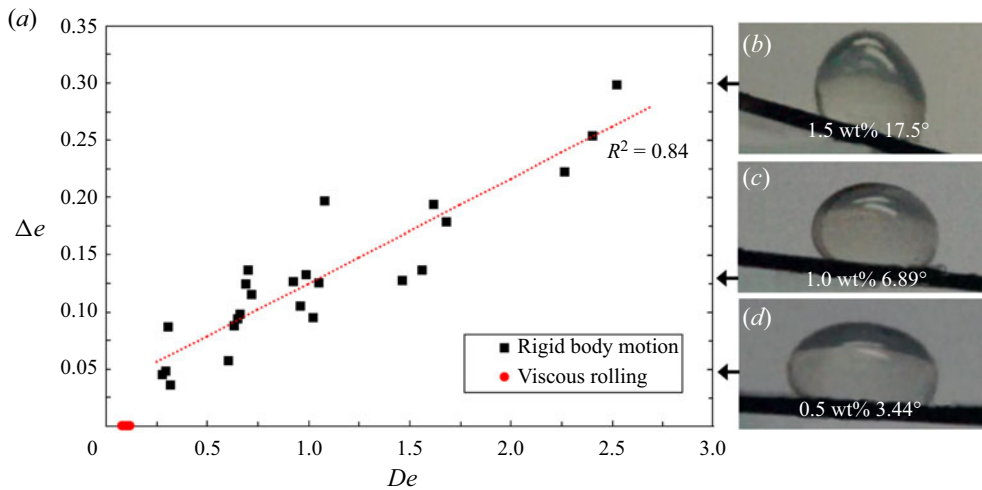


FIGURE 10. (a) Linear relation between Deborah number (De) and eccentricity variation (Δe) in rigid-body motion. The viscous rolling motion does not obey the linear relationship. (b–d) The drop shape at the end of the shape-shifting stage.

represents the velocity difference across the initial height of the drop b (figure 1). After we estimate $\dot{\gamma}_c$ for the moment of shape shifting, the characteristic viscosity η_c is predicted from the power-law relationship of the shear viscosity and the shear rate (figure 3b and table 2) (Macosko 1994). As a result, the Deborah number is presented as follows, and it is expected to be directly proportional to the degree of shape shifting (Δe):

$$De = \frac{t_{relax}}{t_{proc}} \sim \frac{2\eta_c}{(\gamma/b - \sigma_{yield})} \left[\frac{(\sigma_{gra} - \sigma_{yield})}{\rho \pi ab} \right]^{1/2} \sim \Delta e. \quad (3.3)$$

This scaling relation matches well with the experiment as shown in figure 10. The two rolling regimes are separated by a critical De (approximated as 0.2 from figure 10a), and the eccentricity variation for the rigid-body rolling linearly follows De .

It is noteworthy that the time scale for the inclined plane experiments is significantly shorter than that for yielding xanthan gum solutions in the creep tests (e.g. 100 s for 1.5–2.5 wt% in figure 2c–e). Therefore, the shape-shifting and rigid-body motion is thought to be ‘the apparent rheological behaviour’ of the xanthan gum solutions as a ramp of shear rate and/or stress over a short time. Indeed, since the true yield stress of this material was not observed in our experiments, this material is assumed to be an apparent viscoplastic material within the time scale of the observation (i.e. in the inclined plane test).

In this experiment, the rolling velocity of the drop increases even at the end of the substrate and thus the drop motion is not in a steady state. If the released drop had a long enough travel to reach a steady state, it would behave like a viscous Newtonian fluid (i.e. viscous rolling) after the development of an internal flow within the drop and a subsequent decrease in the viscosity (i.e. shear thinning). To identify such transition of the rolling mode, further study is required with a long enough surface.

4. Conclusions

In conclusion, our experimental and theoretical investigation presents the behaviours of a viscoplastic drop on a superhydrophobic surface. Taking advantage of the low surface energy of a superhydrophobic surface, the previously reported complex drop motions were decomposed into three simple motions, i.e. rolling, sliding and sticking. Additionally, two different rolling modes were analysed. If the Deborah number exceeds a critical value, gravity and surface tension conspire to shift the drop shape to be more circular, resulting in rigid-body rolling; whereas typical viscous rolling is observed with lower Deborah number. To the best of our knowledge, this decoupled rolling–sliding–sticking motion and the differentiated rigid-body and viscous rolling of a viscoplastic fluid on a superhydrophobic surface are clear departure from the previous characterizations of Newtonian/non-Newtonian drops.

Supplementary movies

Supplementary movies are available at <https://doi.org/10.1017/jfm.2020.895>.

Acknowledgements

This work was supported by the Climate Change Response Technology Development Project from the National Research Foundation of Korea (NRF-2017M1A2A2047475) and Individual Basic Science & Engineering Research Program from the National Research Foundation of Korea (NRF-2019R1C1C1008262).

Declaration of interests

The authors report no conflict of interest.

REFERENCES

- ANCEY, C. 2007 Plasticity and geophysical flows: a review. *J. Non-Newtonian Fluid Mech.* **142** (1–3), 4–35.
- BALMFORTH, N. J., CRASTER, R. V. & SASSI, R. 2002 Shallow viscoplastic flow on an inclined plane. *J. Fluid Mech.* **470**, 1–29.
- BALMFORTH, N. J., FRIGAARD, I. A. & OVARLEZ, G. 2014 Yielding to stress: recent developments in viscoplastic fluid mechanics. *Annu. Rev. Fluid Mech.* **46**, 121–146.
- BOUJLEL, J. & COUSSOT, P. 2013 Measuring the surface tension of yield stress fluids. *Soft Matter* **9**, 5898–5908.
- CHAMBON, G., GHEMMOUR, A. & NAAIM, M. 2014 Experimental investigation of viscoplastic free-surface flows in a steady uniform regime. *J. Fluid Mech.* **754**, 332–364.
- COUSSOT, P. 2014 Yield stress fluid flows: a review of experimental data. *J. Non-Newtonian Fluid Mech.* **211**, 31–49.
- COUSSOT, P., NGUYEN, Q. D., HUYNH, H. T. & BONN, D. 2002 Avalanche behavior in yield stress fluids. *Phys. Rev. Lett.* **88** (17), 175501.
- COUSSOT, P. & OVARLEZ, G. 2010 Physical origin of shear-banding in jammed systems. *Eur. Phys. J. E* **33**, 183–188.
- DINGKREVE, M., DENN, M. M. & BONN, D. 2017 “Everything flows?”: elastic effects on startup flows of yield stress fluids. *Rheol. Acta* **56**, 189–194.
- DE GENNES, P.-G., BROCHARD-WYART, F. & QUÉRÉ, D. 2013 *Capillarity and Wetting Phenomena: Drops, Bubbles, Pearls, Waves*. Springer Science & Business Media.
- HAO, P., LV, C., YAO, Z. & HE, F. 2010 Sliding behavior of water droplet on superhydrophobic surface. *Europhys. Lett.* **90** (6), 66003.

- HORINAKA, J., TANAKA, M. & TAKIGAWA, T. 2015 Rheological properties of ionic liquid solutions of xanthan. *Colloid Polym. Sci.* **293** (9), 2709–2712.
- HU, B. Y.-K. 2011 Rolling of asymmetric discs on an inclined plane. *Eur. J. Phys.* **32** (6), L51.
- JAISHANKAR, A. & MCKINLEY, G. H. 2014 A fractional K-BKZ constitutive formulation for describing the nonlinear rheology of multiscale complex fluids. *J. Rheol.* **58** (6), 1751–1788.
- JALAAL, M., BALMFORTH, N. J. & STOEBER, B. 2015 Slip of spreading viscoplastic droplets. *Langmuir* **31** (44), 12071–12075.
- JORGENSEN, L., MERRER, M. L., DELANOE-AYARI, H. & BARENTIN, C. 2015 Yield stress and elasticity influence on surface tension measurements. *Soft Matter* **11**, 5111–5121.
- KIM, H. Y., LEE, H. J. & KANG, B. H. 2002 Sliding of liquid drops down an inclined solid surface. *J. Colloid Interface Sci.* **247** (2), 372–380.
- LUU, L. H. & FORTERRE, Y. 2009 Drop impact of yield-stress fluids. *J. Fluid Mech.* **632**, 301–327.
- MACOSKO, C. W. 1994 *Rheology: Principles, Measurements, and Applications*. Wiley-VCH.
- MAHADEVAN, L. & POMEAU, Y. 1999 Rolling droplets. *Phys. Fluids* **11**, 2449–2453.
- MAHAUT, F., CHATEAU, X., COUSSOT, P. & OVARLEZ, G. 2008 Yield stress and elastic modulus of suspensions of noncolloidal particles in yield stress fluids. *J. Rheol.* **52**, 287–313.
- MOLLER, P. C. F., MEWIS, J. & BONN, D. 2006 Yield stress and thixotropy: on the difficulty of measuring yield stresses in practice. *Soft Matter* **2**, 274–283.
- MUSTERD, M., VAN STEIJN, V., KLEIJN, C. R. & KREUTZER, M. T. 2014 Droplets on inclined plates: local and global hysteresis of pinned capillary surfaces. *Phys. Rev. Lett.* **113** (6), 066104.
- OISHI, C. M., THOMPSON, R. L. & MARTINS, F. P. 2019 Normal and oblique drop impact of yield stress fluids with thixotropic effects. *J. Fluid Mech.* **876**, 642–679.
- OVARLEZ, G., COHEN-ADDAD, S., KRISHAN, K., GOYON, J. & COUSSOT, P. 2013 On the existence of a simple yield stress fluid behavior. *J. Non-Newtonian Fluid Mech.* **193**, 68–79.
- PODGORSKI, T., FLESSELLES, J. M. & LIMAT, L. 2001 Corners, cusps, and pearls in running drops. *Phys. Rev. Lett.* **87** (3), 036102.
- REINER, M. 1964 The Deborah number. *Phys. Today* **17** (1), 62.
- RICHARD, D. & QUÉRÉ, D. 1999 Viscous drops rolling on a tilted non-wettable solid. *Europhys. Lett.* **48** (3), 286–291.
- RIO, E., DAERR, A., ANDREOTTI, B. & LIMAT, L. 2005 Boundary conditions in the vicinity of a dynamic contact line: experimental investigation of viscous drops sliding down an inclined plane. *Phys. Rev. Lett.* **94** (2), 024503.
- SAKAI, M., SONG, J. H., YOSHIDA, N., SUZUKI, S., KAMESHIMA, Y. & NAKAJIMA, A. 2006 Direct observation of internal fluidity in a water droplet during sliding on hydrophobic surfaces. *Langmuir* **22** (11), 4906–4909.
- SCELLENBERGER, F., ENCINAS, N., VOLLMER, D. & BUTT, H. J. 2016 How water advances on superhydrophobic surfaces. *Phys. Rev. Lett.* **116** (9), 096101.
- SEN, S., MORALES, A. G. & EWOLDT, R. H. 2020 Viscoplastic drop impact on thin films. *J. Fluid Mech.* **891**, A27.
- SEO, K., KIM, M. & KIM, D. H. 2014 Candle-based process for creating a stable superhydrophobic surface. *Carbon* **68**, 583–596.
- SEO, K., KIM, M., SEOK, S. & KIM, D. H. 2016 Transparent superhydrophobic surface by silicone oil combustion. *Colloids Surf. A* **492**, 110–118.
- SONG, K. W., KIM, Y.-S. & CHANG, G.-S. 2006 Rheology of concentrated xanthan gum solutions: steady shear flow behavior. *Fibers Polym.* **7** (2), 129–138.
- SUZUKI, S., NAKAJIMA, A., SAKAI, M., SAKURADA, Y., YOSHIDA, N., HASHIMOTO, A., KAMESHIMA, Y. & OKADA, K. 2007 Slipping and rolling ratio of sliding acceleration for a water droplet sliding on fluoroalkylsilane coatings of different roughness. *Chem. Lett.* **37** (1), 58–59.
- VARAGNOLO, S., FERRARO, D., FANTINEL, P., PIERNO, M., MISTURA, G., AMATI, G., BIFERALE, L. & SBRAGAGLIA, M. 2013 Stick-slip sliding of water drops on chemically heterogeneous surfaces. *Phys. Rev. Lett.* **111** (6), 066101.
- VARAGNOLO, S., MISTURA, G., PIERNO, M. & SBRAGAGLIA, M. 2015 Sliding droplets of xanthan solutions: a joint experimental and numerical study. *Eur. Phys. J. E* **38** (11), 126.
- WHISTLER, R. L. & BEMILLER, J. N. 1993 *Industrial Gums*. Academic Press.

- WYATT, N. B. & LIBERATORE, M. W. 2009 Rheology and viscosity scaling of the polyelectrolyte xanthan gum. *J. Appl. Polym.* **114** (6), 4076–4084.
- ZHANG, X., LORENCEAU, E., BASSET, P., BOUROUINA, T., ROUYER, F., GOYON, J. & COSSOT, P. 2017 Wall slip of soft-jammed systems: a generic simple shear process. *Phys. Rev. Lett.* **119** (20), 208004.
- ZHANG, X., LORENCEAU, E., BOUROUINA, T., BASSET, P., OERTHER, T., FERRARI, M., ROUYER, F., GOYON, J. & COUSSOT, P. 2018 Wall slip mechanisms in direct and inverse emulsions. *J. Rheol.* **62**, 1495–1513.